IOP Publishing

Eugene Oks

Appendix A

Overview of the theories of the dynamical Stark broadening of ion spectral lines in plasmas

Here we limit the presentation by the dynamical Stark broadening of hydrogenlike ion lines by plasma electrons. It was initially developed by Griem and Shen [1] (see also books [2, 3]). It is often called the conventional theory (CT); sometimes it is called the standard theory.

The dynamical broadening of spectral lines in plasmas by electrons is effective if the number ν_{We} of perturbing electrons in the sphere of the electron Weisskopf radius ρ_{We} is much smaller than unity (see, e.g. review [4]): $\nu_{We} = 4\pi N_e \rho_{We}^3/3 \ll 1$, where N_e is the electron density and $\rho_{We} \sim n^2\ \hbar/(m_e v_{Te})$. Here n is the principal quantum number of the radiator energy level involved in the radiative transition and v_{Te} is the mean thermal velocity of plasma electrons. Under this condition, for the overwhelming majority of perturbing electrons, the characteristic frequency of the variation of the electron microfield $\Omega_e \sim v_{Te}/\rho_{We}$ is much greater than the instantaneous Stark splitting in the electron microfield. Physically, the electron Weisskopf radius is related to the impact parameters $\rho \sim \rho_{We}$ that contribute most effectively to the dynamical Stark broadening of spectral lines by electrons in plasmas [4].

The gist of dynamical effects in the Stark broadening of spectral lines in plasmas by electrons is the following. Collisions with plasma electrons cause *virtual transitions* mostly within the upper (n) and lower (n') multiplets during the radiative transition $n \leftrightarrow n'$. The primary outcome is a *decrease of the lifetime* of the states n' and/or n of the radiator, thus leading to the broadening of the corresponding spectral line.

The fact that virtual transitions occur mostly within the upper and lower multiplets conventionally leads to so-called *no-quenching approximation*, in which virtual transitions between states of different principal quantum numbers are totally disregarded. This approximation allows introducing the so-called *line space*: a direct product of the Hilbert space, spanned on the basis vectors of the n-shell, with the Hilbert space, spanned on the (complex-conjugated) basis vectors of the n'-shell.

doi:10.1088/978-0-7503-3375-7ch7

The origin of the CT can be traced back to the impact formalism developed by Baranger [5] and then by Kolb and Griem [6]. The central point of the impact formalism is the employment of a *coarse-grained time scale* Δt. Namely, on the one hand, Δt should be chosen such that it is much greater than the characteristic time ρ/v of the variation of the electric field created by the perturbing electron at the location of the radiating ion. Here ρ is the impact parameter and v is the velocity of the perturbing electron. On the other hand, Δt should be chosen such that it is much smaller than $[\max(\gamma, \Delta\omega, \omega_{\mathrm{pe}})]^{-1}$. Here γ is the inversed lifetime of the radiator (the impact width of the spectral line is of the order of γ), $\Delta\omega$ is the detuning from the unperturbed frequency ω_0 of the spectral line, $\omega_{\mathrm{pe}} = (4\pi N_e e^2/m_e)^{1/2}$ is the plasma electron frequency.

Physically, the coarse-grained time scale means that we are not interested in details of the evolution of the radiator during the characteristic time of the individual collision ρ/v. Instead, we are interested in the evolution of the radiator during larger time intervals Δt. The limits of validity of the impact approximation are controlled by the introduction of the coarse-grained time.

For completeness we should mention the so-called unified formalism developed by Vidal, Cooper, and Smith [7]. The primary distinction of the unified formalism from the impact formalism is the following. The *impact* formalism considers only *completed collisions*, while the *unified* formalism allows also for *incomplete collisions*. Another difference relates to the fact that the unified formalism allows (at least in principle) a transition to the nearest-neighbor quasistatic result in the wings of the spectral line. This difference is less important: quantitatively the unified formalism does not always produce such transition correctly. It should be noted that one of the conditions for introducing the coarse-grain time scale is somewhat relaxed in the unified formalism compared to the impact formalism. Namely, in the unified formalism it is required that $\rho/v \leqslant \Delta t$—compared to the requirement $\rho/v \ll \Delta t$ in the impact formalism. Further details on the rigorous description of both formalisms can be found in the comprehensive review by Sahal-Brechot [8].

The CT leads to the expression for the so-called electron impact broadening operator containing a diverging integral: the integral over the impact parameters. This integral diverges at both small and large impact parameters. This divergence is one of the primary deficiencies of the CT.

The divergence at large ρ is related to the long-range nature of the Coulomb potential. There occurs the plasma screening of the electric field of the perturbing electron at the distances larger than the Debye radius

$$\rho_D = [T_e/(^4pe^2N_e)]^{1/2} \tag{A.1}$$

where T_e is the electron temperature. This leads to choosing the upper cutoff at $\rho_{\max} \sim \rho_D$. In distinction, the divergence at small impact parameters in the CT is due the employment of the perturbation expansion.

The above deficiency of the CT has been eliminated with the development of the so-called generalized theory (GT) of the dynamical Stark broadening of hydrogenic

spectral lines [9, 10] (see also book [11]). The GT is based on a *generalization* of the formalism of dressed atomic states (DAS) in plasmas.

Originally the DAS-formalism was introduced for studies of the interaction of a *monochromatic* (or quasi-monochromatic) field—such as, for example, laser or maser radiation—with gases. In the course of further research, the DAS-formalism was extended to the description of the interaction of a laser or maser radiation with plasmas [12]. This resulted in more accurate analytical calculations and better (more robust) codes.

The *generalization* of DAS in papers [9, 10] was based on utilizing atomic states dressed not by a monochromatic field, but by a *broad-band* field of plasma electrons and ions. As should be expected, the generalized DAS is a more complex concept than the usual DAS.

Due to the utilization of the generalized DAS, the authors of papers [9, 10] succeeded in taking into account analytically a *coupling* of the electron and ion microfields facilitated by the radiating atom. This coupling increases with the growth of the principal quantum number n and with the growth of the electron density N_e, as well as with the decrease of the temperature T.

We mention in passing that some of the later extensions of the GT caused some discussions in the literature. However, the core GT developed in papers [9, 10] has stood the test of time.

The GT eliminated large discrepancies—up to a factor of two—between the CT and benchmark experiments, as presented in part of book [11]. Below are some more details on the GT.

The Hamiltonian of a hydrogenic atom or ion subjected to the quasistatic part $\mathbf{F}$ of the ion microfield and to the electron-produced dynamic field $\mathbf{E}(t)$ can be represented in the form

$$H = H_0 - \mathbf{dF} - \mathbf{dE}(t), \tag{A.2}$$

where H_0 is the unperturbed Hamiltonian, $\mathbf{d}$ is the dipole moment operator. One chooses the axis Oz of the parabolic quantization along the field $\mathbf{F}$. Then the operator—$\mathbf{dF}$ is diagonal in any subspace of a fixed principal quantum number n. For this reason, in the CT this interaction was taken into account 'exactly' (neglecting only some corrections due to the matrix elements of the operator d_z corresponding to $\Delta n \neq 0$). The interaction with the field $\mathbf{E}(t)$ in the CT was subsequently treated in the second order of the Dirac's (time-dependent) perturbation theory.

In distinction, in the GT, the entire z-component of the total field $\mathbf{F} + \mathbf{E}(t)$ is allowed for in the same (or analogous) way as the field $\mathbf{F}$ was treated in the CT. This was possible because the interaction $-d_z[F + E_z(t)]$ (and not only its part $-d_zF$) is diagonal in any n-subspace. Therefore, the z-component of the electron microfield can be taken into account much more accurately than in the CT. In this way, the Stark sublevels are *dynamically dressed* by the entire z-component of the total microfield $\mathbf{F} + \mathbf{E}(t)$. This is the central feature of the GT that leads to its several advantages over the CT.

In the GT electron broadening operator and in the GT correlation function, whose Fourier transform is the lineshape, there are adiabatic and nonadiabatic terms. The adiabatic term in the correlation function is proportional to the part $d_z d_z$ of the operator **dd**; the operator $d_z d_z$ is diagonal in the line space (we recall that the line space is the Gilbert space spanned on the upper and lower Stark substates involved in the radiative transition). The rest of the correlation function corresponds to the non-adiabatic contribution: it is proportional to the operator $d_x d_x + d_y d_y$ that has both diagonal and non-diagonal matrix elements in the line space.

In the GT, the adiabatic part of the electron broadening operator and of the correlation function is calculated *exactly*. This exact result is equivalent to the summation of all orders of the corresponding Dyson expansion entering formulas of both the CT and the GT. This is one of the most important distinctions from the CT, where all terms in the electron broadening operator and of the correlation function are calculated only in the first non-vanishing (namely, the second) order of the Dyson expansion.

As a result, the GT is *convergent* at small impact parameters while the corresponding CT for neutral radiators is divergent. (For charged radiators the CT is formally convergent, but leads quantitatively to wrong results.) It is the allowance for the 'dressing' by the broad band field $F + E_z(t)$ that eliminates the divergence and enhances the accuracy of the results. In distinction, the higher the electron density and/or the principal quantum number (or the lower the temperature), the greater becomes the inaccuracy of the CT.

It should be noted that the GT was developed *analytically* to the same level as the CT. This is counterintuitive because the starting formulas for the GT are more complicated than for the CT.

Speaking specifically about the dynamical Stark broadening of hydrogenlike spectral lines by plasma electrons, there is another fundamental flaw of the CT. This flaw has been eliminated in paper [13] (see also chapter 12 of book [14]), which we follow below.

In the CT, the perturbing electrons are considered moving along hyperbolic trajectories in the Coulomb field of the effective charge $Z - 1$ (in atomic units), where Z is the nuclear charge of the radiating ion. In other words, in the CT there was made a simplifying assumption that the motion of the perturbing electron can be described in frames of a two-body problem, one particle being the perturbing electron and the other 'particle' being the charge $Z - 1$.

However, in reality one has to deal with a three-body problem: the perturbing electron, the nucleus, and the bound electron. Therefore, trajectories of the perturbing electrons should be more complicated.

In paper [13] the authors took this into account by using the standard analytical method of separating rapid and slow subsystems—see, e.g. book [15]. The characteristic frequency of the motion of the bound electron around the nucleus is much higher than the characteristic frequency of the motion of the perturbing electron around the radiating ion. Therefore, the former represents the rapid subsystem and the latter represents the slow subsystem. This approximate analytical method allows

a sufficiently accurate treatment in situations where the perturbation theory fails—see, e.g. book [15].

By applying this method the authors of paper [13] obtained more accurate analytical results for the electron broadening operator than in the CT. They showed by examples of the electron broadening of the Lyman lines of He II that the allowance for this effect increases with the electron density N_e, becomes significant already at $N_e \sim 10^{17}$ cm^{-3} and very significant at higher densities. Below are the details.

In the CT the electron broadening operator is expressed in the form (see, e.g. paper [1])

$$\Phi_{ab} \equiv 2\pi v N_e \int d\rho\, \rho\{S_a S_b^* - 1\}, \tag{A.3}$$

where N_e, v, and ρ are the electron density, velocity, and impact parameter, respectively; $S_a(0)$ and $S_b(0)$ are the S matrices for the upper (a) and lower (b) states involved in the radiative transition, respectively; $\{\ldots\}$ stands for the averaging over angular variables of vectors **v** and **ρ**. Further in the CT, the collisions are subdivided into weak and strong. The weak collisions are treated by the time-dependent perturbation theory. The impact parameter, at which the formally calculated expression $\{S_a S_b^* - 1\}$ for a weak collision starts violating the unitarity of the S-matrices, serves as the boundary between the weak and strong collisions and is called Weisskopf radius ρ_{We}.

So, in the CT the integral over the impact parameter diverges at small ρ. Therefore, in the CT this integral is broken down into two parts: from 0 to ρ_{We} (strong collisions) and from ρ_{We} to $\rho_{\max}$ for weak collisions. The upper cutoff $\rho_{\max}$ (typically chosen to be the Debye radius given by equation (A.1)) is necessary because this integral diverges also at large ρ.

In the CT, after calculating the S matrices for weak collisions, the electron broadening operator becomes (*in atomic units*)

$$\Phi_{ab}{}^{\text{weak}} \equiv C \int_{\rho_{we}}^{\rho_{\max}} d\rho\, \rho \sin^2 \frac{\Theta(\rho)}{2} = \frac{C}{2} \int_{\Theta_{\min}}^{\Theta_{\max}} d\Theta \frac{d\rho^2}{d\Theta} \sin^2 \frac{\Theta}{2}, \tag{A.4}$$

where Θ is the scattering angle for the collision between the perturbing electron and the radiating ion (the dependence between Θ and ρ being discussed below) and the plasma electron and the operator C is

$$C = -\frac{4\pi}{3} N_e \left[\int_0^\infty dv v^3 f(v)\right] \frac{m^2}{(Z-1)^2} (\boldsymbol{r}_a - r_b^*)^2. \tag{A.5}$$

Here $f(v)$ is the velocity distribution of the perturbing electrons, $\boldsymbol{r}$ is the radius-vector operator of the bound electron (which scales with Z as $1/Z$), and m is the reduced mass of the system 'perturbing electron—radiating ion'.

In the CT the scattering occurs in the effective Coulomb potential, so that the trajectory of the perturbing electron is hyperbolic and the relation between the impact parameter and the scattering angle is given by

$$\rho^{(0)} = \frac{Z-1}{mv^2}\cot\frac{\Theta}{2}. \tag{A.6}$$

In paper [13] the authors considered the realistic situation where trajectories of the perturbing electrons are more complicated because the perturbing electron, the nucleus, and the bound electron should be more accurately treated as the three-body problem. We use the standard analytical method of separating rapid and slow subsystems—see, e.g. book [15]. It is applicable here because the characteristic frequency $v_{\mathrm{Te}}/\rho_{We}$ of the variation the electric field of the perturbing electrons at the location of the radiating ion is much smaller than the frequency Ω_{ab} of the spectral line (the latter, e.g. in case of the radiative transition between the Rydberg states would be the Keppler frequency or its harmonics)—more details on this are presented at the end of this chapter.

The first step in this method is to 'freeze' the slow subsystem (perturbing electron) and to find the analytical solution for the energy of the rapid subsystem (the radiating ion) that would depend on the frozen coordinates of the slow subsystem (in our case it will be the dependence on the distance R of the perturbing electron from the radiating ion). To the first non-vanishing order of the R-dependence, the corresponding energy in the parabolic quantization is given by

$$E_{nq}(R) = -\frac{Z^2}{n^2} + \frac{3\,nq}{2\,ZR^2}, \tag{A.7}$$

where n and $q = n_1 - n_2$ are the principal and electric quantum numbers, respectively; n_1 and n_2 are the parabolic quantum numbers.

The next step in this method is to consider the motion of the slow subsystem (perturbing electron) in the 'effective potential' $v_{\mathrm{eff}}(R)$ consisting of the actual potential plus $E_{nq}(R)$. Since the constant term in equation (A.7) does not affect the motion, the effective potential for the motion of the perturbing electron can be represented in the form

$$V_{\mathrm{eff}}(R) = -\frac{\alpha}{R} + \frac{\beta}{R^2}, \;\; \alpha = Z - 1. \tag{A.8}$$

For the spectral lines of the Lyman series, since the lower (ground) state b of the radiating ion remains unperturbed (up to/including the order $\sim 1/R^2$), the coefficient β is

$$\beta = \frac{3\,n_a q_a}{2\,Z}. \tag{A.9}$$

For other hydrogenic spectral lines, for taking into account both the upper and lower states of the radiating ion, the coefficient β can be expressed as

$$\beta = \frac{3\,(n_a q_a - n_b q_b)}{2\,Z}. \tag{A.10}$$

The motion in the potential from equation (A.8) allows an exact analytical solution. In particular, the relation between the scattering angle and the impact parameter is no longer given by equation (A.6), but rather becomes (see, e.g. book [16])

$$\Theta = \pi - \frac{2}{\sqrt{1 + \frac{2\,m\beta}{M^2}}} \arctan \sqrt{\frac{4\,E}{\alpha^2}\left(\beta + \frac{M^2}{2m}\right)}. \tag{A.11}$$

Here E and M are the energy and the angular momentum of the perturbing electron, respectively. One can rewrite the angular momentum in terms of the impact parameter ρ as

$$M = mv\rho \tag{A.12}$$

Then a slight rearrangement of equation (A.11) yields

$$\tan\left(\frac{\pi - \Theta}{2}\sqrt{1 + \frac{2\,\beta}{mv^2\rho^2}}\right) = \frac{v}{\alpha}\sqrt{m^2v^2\rho^2 + 2\,m\beta}\,. \tag{A.13}$$

After solving equation (A.13) for ρ and substituting the outcome in equation (A.4), a more accurate expression for the electron broadening operator can be obtained. However, equation (A.13) does not have an exact analytic solution for ρ so that this could be done only numerically.

In paper [13], for getting the message across in the simplest form, the authors provided an approximate analytical solution of equation (A.13) by expanding it in powers of β. This yields (keeping up to the first power of β)

$$\tan\left(\frac{\pi - \Theta}{2}\right) + \left(\frac{\pi - \Theta}{2}\right)\left[1 + \tan^2\left(\frac{\pi - \Theta}{2}\right)\right]\frac{\beta}{mv^2\rho^2} \approx \frac{mv^2\rho}{\alpha} + \frac{\beta}{\alpha\rho}. \tag{A.14}$$

The authors of paper [13] were seeking the analytical solution for ρ in the form $\rho \approx \rho^{(0)} + \rho^{(1)}$, where $\rho^{(0)}$ corresponds to $\beta = 0$ (and was given by equation (A.6)) and $\rho^{(1)} \ll \rho^{(0)}$. Substitution of $\rho \approx \rho^{(0)} + \rho^{(1)}$ into equation (A.14) yields the expression

$$\frac{(\pi - \Theta)\,\beta}{2\,mv^2\rho^{(0)2}\sin^2\frac{\Theta}{2}} - \frac{\beta}{\alpha\rho^{(0)}} \approx \frac{mv^2\rho^{(1)}}{\alpha}. \tag{A.15}$$

After solving equation (A.15) for $\rho^{(1)}$, one gets the expression for ρ:

$$\rho \approx \frac{\alpha}{mv^2}\cot\frac{\Theta}{2} + \frac{\beta}{\alpha}\left(\frac{\pi - \Theta}{2\cos^2\frac{\Theta}{2}} - \tan\frac{\Theta}{2}\right). \tag{A.16}$$

As a reminder, the goal is to perform the integration in equation (A.3) for obtaining a more accurate analytical result for the electron broadening operator. This can be more easily accomplished by performing the integration over Θ instead of ρ. For this purpose, first, the authors of paper [13] squared equation (A.16)

$$\rho^2 \approx \frac{\alpha^2}{m^2 v^4}\cot^2\frac{\Theta}{2} + \frac{\beta}{mv^2}\left(\frac{\pi-\Theta}{\sin\frac{\Theta}{2}\cos\frac{\Theta}{2}} - 1\right), \tag{A.17}$$

where only the first order terms in β have been kept for consistency. To make formulas simpler, they denoted $\phi = \Theta/2$. After differentiating equation (A.17) with respect to ϕ, the authors of paper [13] obtained

$$\frac{d\rho^2}{d\phi} \approx -\frac{\alpha^2}{m^2 v^4}\frac{2\cot\phi}{\sin^2\phi} - \frac{2\beta}{mv^2}\left[\left(\frac{1}{\sin\phi\cos\phi}\right) + \left(\frac{\pi}{2}-\phi\right)\left(\frac{1}{\sin^2\phi} - \frac{1}{\cos^2\phi}\right)\right]. \tag{A.18}$$

After substituting in the utmost right side of equation (A.4) first $\Theta = 2\phi$ and then $\frac{d\rho^2}{d\phi}$ from equation (A.18), the contribution of the weak collisions to the electron broadening operator becomes

$$\begin{aligned}\Phi_{ab}{}^{\text{weak}} = -C\Bigg[&\frac{\alpha^2}{m^2 v^4}\int_{\phi_{\min}}^{\phi_{\max}}\cot\phi\, d\phi + \frac{\beta}{mv^2}\int_0^{\frac{\pi}{2}}\tan\phi\, d\phi \\ &+ \frac{\beta}{mv^2}\int_0^{\frac{\pi}{2}}\left(\frac{\pi}{2}-\phi\right)(1-\tan^2\phi)d\phi\Bigg].\end{aligned} \tag{A.19}$$

In equation (A.19), in the two correction terms proportional to β, The authors of paper [13] extended the integration over the full range of the variation of the angle ϕ. The corresponding minor inaccuracy would not contribute significantly to the electron broadening operator, since the terms involving β are considered to be a relatively small correction to the first term in equation (A.19).

Performing the integrations in equation (A.19), they obtained:

$$\begin{aligned}\Phi_{ab}{}^{\text{weak}} = -\frac{4\pi}{3}N_e(\mathbf{r}_a - r_b^*)^2\left[\int_0^\infty dv\frac{f(v)}{v}\right] \\ \times\left[\log\frac{\sin\phi_{\max}}{\sin\phi_{\min}} + \frac{mv^2\beta}{(Z-1)^2}\left(\frac{\pi^2}{4}-1\right)\right].\end{aligned} \tag{A.20}$$

Here and below the expression $(\mathbf{r}_a - \mathbf{r}_b^*)^2$ stands for the scalar product (also known as the dot-product) of the operator $(\mathbf{r}_a - \mathbf{r}_b^*)$ with itself. In the theory of the dynamical Stark broadening of spectral lines in plasmas by electrons, the corresponding matrix elements are calculated with respect to the unperturbed wave functions.

Then the authors of paper [13] added the CT estimate for the contribution of strong collisions

$$\Phi_{ab}{}^{\text{strong}} \approx \pi v N_e \rho_{We}{}^2, \tag{A.21}$$

where ρ_{We} corresponds to $\phi_{\max}$. Expressions for $\phi_{\max}$ and $\phi_{\min}$ are given in paper [1] (in equations (9) and (10a)) as follows

$$\sin\phi_{\max} = \sqrt{\frac{3}{2}}\frac{Z(Z-1)}{(n_a^2 - n_b^2)mv}, \tag{A.22}$$

$$\sin\phi_{\min} = \frac{\frac{Z-1}{mv^2\rho_D}}{\sqrt{1+\frac{(Z-1)^2}{m^2v^4\rho_D^2}}} \tag{A.23}$$

It should be emphasized that the factor $(n_a^2 - n_b^2)$ in the denominator of the right side of equation (A.22) was an approximate allowance by the authors of paper [1] for the contribution of the lower level b while estimating the operator $(\boldsymbol{r}_a - r_b^*)$ for hydrogenic lines of spectral series other than the Lyman lines. However, for the Lyman lines the lower (ground) level does not contribute to electron broadening operator, so that for the Lyman lines equation (A.22) should be simplified as follows:

$$\sin\phi_{\max} = \sqrt{\frac{3}{2}}\frac{Z(Z-1)}{n_a^2 mv}. \tag{A.24}$$

It should be noted that at relatively small velocities of perturbing electrons, the right side of equation (A.22) or equation (A.24) could exceed unity. In this case one should set $\sin\phi_{\max} = 1$, what corresponds to $\rho_{\min} = 0$, so that there would be no contribution from strong collisions. Typically, the range of such small velocities has a very low statistical weight in the electron velocity distribution.

After substituting the above formulas for $\sin\phi_{\max}$ and $\sin\phi_{\min}$ into equation (A.19), and combining the contributions from weak and strong collisions, the authors of paper [13] obtained the final results for the electron broadening operator:

$$\begin{aligned}\Phi_{ab}(\beta) = &-\frac{4\pi}{3}N_e(\boldsymbol{r}_a - r_b^*)^2\left[\int_0^\infty dv\frac{f(v)}{v}\right]\left\{\frac{1}{2}\left[1 - \frac{3}{2}\frac{Z^2(Z-1)^2}{(n_a^2 - n_b^2)^2 m^2v^2}\right]\right.\\ &\left.+\log\left[\sqrt{\frac{3}{2}}\frac{Zv\rho_D}{(n_a^2 - n_b^2)}\sqrt{1+\left(\frac{Z-1}{mv^2\rho_D}\right)^2}\right] + \frac{mv^2\beta}{(Z-1)^2}\left(\frac{\pi^2}{4} - 1\right)\right\}\end{aligned} \tag{A.25}$$

for the non-Lyman lines and

$$\begin{aligned}\Phi_{ab}(\beta) = &-\frac{4\pi}{3}N_e(\boldsymbol{r}_a - r_b^*)^2\left[\int_0^\infty dv\frac{f(v)}{v}\right]\left\{\frac{1}{2}\left[1 - \frac{3}{2}\frac{Z^2(Z-1)^2}{n_a^4 m^2v^2}\right]\right.\\ &\left.+\log\left[\sqrt{\frac{3}{2}}\frac{Zv\rho_D}{n_a^2}\sqrt{1+\left(\frac{Z-1}{mv^2\rho_D}\right)^2}\right] + \frac{mv^2\beta}{(Z-1)^2}\left(\frac{\pi^2}{4} - 1\right)\right\}\end{aligned} \tag{A.26}$$

for the Lyman lines. Here and below log[…] stands for the natural logarithm.

In order to determine the significance of this effect, it is necessary then to evaluate the ratio

$$\text{ratio} = \frac{\frac{3}{2}\frac{mv^2(n_a q_a - n_b q_b)}{(Z-1)^2}\left(\frac{\pi^2}{4} - 1\right)}{\frac{1}{2}\left[1 - \frac{3}{2}\frac{Z^2(Z-1)^2}{\left(n_a^2 - n_b^2\right)^2 m^2 v^2}\right] + \log\left[\sqrt{\frac{3}{2}}\frac{Zv\rho_D}{\left(n_a^2 - n_b^2\right)}\sqrt{1 + \left(\frac{Z-1}{mv^2\rho_D}\right)^2}\right]} \tag{A.27}$$

for the non-Lyman lines or the ratio

$$\text{ratio} = \frac{\frac{3}{2}\frac{mv^2 n_a q_a}{(Z-1)^2}\left(\frac{\pi^2}{4} - 1\right)}{\frac{1}{2}\left[1 - \frac{3}{2}\frac{Z^2(Z-1)^2}{n_a^4 m^2 v^2}\right] + \log\left[\sqrt{\frac{3}{2}}\frac{Zv\rho_D}{n_a^2}\sqrt{1 + \left(\frac{Z-1}{mv^2\rho_D}\right)^2}\right]} \tag{A.28}$$

for the Lyman lines.

Below we reproduce numerical examples for several Lyman lines from paper [13]. As is customary in the Stark broadening theory, instead of the integration over velocities, for the numerical examples the authors of paper [13] used the mean thermal velocity v_T of the perturbing electrons. In atomic units, the mean thermal velocity v_T, the Debye radius ρ_D, and the reduced mass can be expressed as follows

$$v_T = 0.1917\sqrt{\frac{T(\text{eV})}{m}}\rho_D = 1.404 \times 10^{11}\sqrt{\frac{T(\text{eV})}{N_e(\text{cm}^{-3})}}m = \frac{1 + \frac{m_e}{Am_p}}{1 + \frac{2\,m_e}{Am_p}}, \tag{A.29}$$

where m_e is the electron mass, m_p is the proton mass, and A is the atomic number of the radiating ion ($A \approx 2Z$).

Table A1 presents the values of the ratio from equation (A.28) for several Lyman lines of He II at the temperature $T = 8$ eV and the electron density $N_e = 2 \times 10^{17}$ cm^{-3}.

Figure A1 shows the ratio from equation (A.28) versus the electron density N_e for the Stark components of the electric quantum number $|q| = 1$ of Lyman-alpha ($n = 2$), Lyman-beta ($n = 3$), and Lyman-gamma ($n = 4$) lines of He II at the temperature $T = 8$ eV.

It is seen that for the electron broadening of the Lyman lines of He II, the allowance for the effect under consideration indeed becomes significant already at electron densities $N_e \sim 10^{17}$ cm^{-3} and increases with the growth of the electron density. It should be noted that when the ratio, formally calculated by equation (A.28), becomes comparable to unity, this is the indication that the approximate analytical treatment based on expanding equation (A.13) up to the first order of parameter β, is no longer valid. In this case the calculations should be based on solving equation (A.13) with respect to ρ without such approximation.

Table A1. Ratio from equation (A.28) for the Stark components of several Lyman lines of He II. at the temperature $T = 8$ eV and the electron density $N_e = 2 \times 10^{17}$ cm^{-3} [13].

n	$\|q\|$	*ratio*
2	1	0.3261
3	1	0.3748
3	2	0.7496
4	1	0.5156
4	2	1.0311
4	3	1.5467

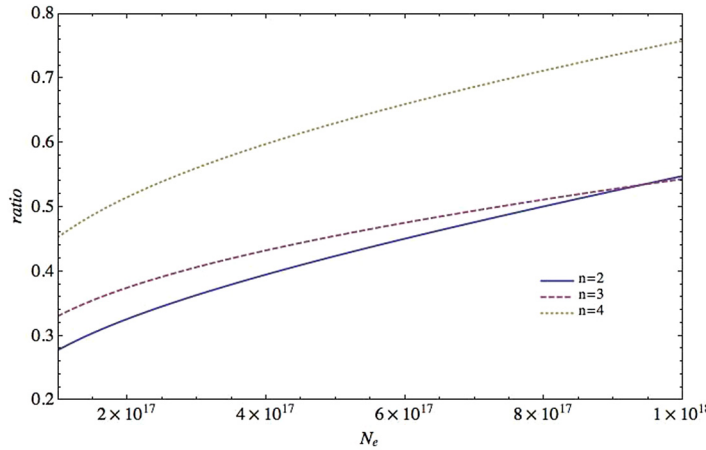

Figure A1. Ratio from equation (A.28) versus the electron density N_e for the Stark components of the electric quantum number $|q| = 1$ of Lyman-alpha ($n = 2$), Lyman-beta ($n = 3$), and Lyman-gamma ($n = 4$) lines of He II at the temperature $T = 8$ eV [13].

Thus, the authors of paper [13] obtained more accurate analytical results for the electron broadening operator compared to the CT. By examples of the electron broadening of the Lyman lines of He II, we demonstrated that the allowance for this effect becomes significant at electron densities $N_e \sim 10^{17}$ cm^{-3} and very significant at higher densities. It is well-known that for relatively low-Z radiators, the broadening by electrons is comparable to the broadening by ions, so that the correction to the broadening by electrons, introduced in the present paper, should be significant for the total Stark width.

It is important to emphasize that the authors of paper [13] were able to obtain the above analytical results primarily due to the underlying fundamental symmetry of the class of potentials $v(R) = -A/R + B/R^2$, where A and B are constants. Namely, this class of potentials possesses an additional conserved quantity $M_{\text{eff}}{}^2 = M^2 +$

$2mB$, where M is the angular momentum and m is the mass of a particle, so that M_{eff} is the effective angular momentum. As for the impact approximation, it was not crucial to work [13]—the authors used it only for the following two purposes: first, to get the message across in a simple form, and second, for the comparison with the CT (in which the impact approximation was crucial), so that we would compare 'apples to apples' rather than 'apples to oranges'.

The authors of paper [13] also mentioned that in 1981, Baryshnikov and Lisitsa [17] published very interesting results for the electron broadening of hydrogen-like spectral lines in plasmas (also presented later in book [18]) in frames of the quantum theory of the dynamical Stark broadening, while we obtained our results in frames of the semiclassical theory of the dynamical Stark broadening, just as in the CT. (For clarity: in the semiclassical theory, the radiating atom/ion is treated quantally, and perturbing electrons classically; in the quantum theory both the radiating atom/ion and perturbing electrons are treated quantally.) Both in paper [17] and in paper [13], there was used the underlying symmetry of the class of potentials $v(R) = -A/R + B/R^2$ for obtaining analytical solutions.

A specific result for the line width Baryshnikov and Lisitsa [17] obtained for Lyman lines in the classical limit using the impact approximation, as presented in their equations (4.5) and (4.6). The authors of paper [13] compared their results from equations (4.5) and (4.6) with the CT [1] for He II Lyman lines. It turned out that for $N_e \sim (10^{17}$–$10^{18})$ cm^{-3}, i.e. for the range of electron densities, in which the overwhelming majority of measurements of the width of He II lines were performed, Baryshnikov–Lisitsa's line width exceeds the CT line width by two orders of magnitude or more. In view of the fact that the width of He II lines, measured by various authors in benchmark experiments (i.e. experiments where plasma parameters were measured independently of the line widths), never exceeded the CT width by more than a factor of two (see, e.g. benchmark experiments [19–21]), this seems to indicate that something might be incorrect in equations (4.5) and (4.6) from paper [17] (though methodologically it was a very interesting paper). In distinction, the corrections to the CT introduced in paper [13], do not exceed the factor of two for He II lines in the range of $N_e \sim (10^{17}$–$10^{18})$ cm^{-3}.

Finally, the authors of paper [13] provided a detailed proof of the applicability of the analytical method (that they used) as follows. The characteristic frequency of the motion of the perturbing electron around the radiating ion in the process of the Stark broadening of spectral lines is the so-called Weisskopf frequency

$$\omega_{We} = \frac{v_T}{\rho_{We}} \sim \frac{Zmv_T^2}{(n_a^2 - n_b^2)\hbar} \sim \frac{ZT}{(n_a^2 - n_b^2)\hbar}. \tag{A.30}$$

The characteristic frequency of the motion of the bound electron around the nucleus is the frequency of the spectral line

$$\Omega = \frac{Z^2 U_H}{\hbar}\left(\frac{1}{n_b^2} - \frac{1}{n_a^2}\right), \tag{A.31}$$

where U_H is the ionization potential of hydrogen. The ratio of these two frequencies is

$$\frac{\omega_{We}}{\Omega} \sim \left(\frac{T}{ZU_H}\right)\left[\frac{n_a^2 n_b^2}{\left(n_a^2 - n_b^2\right)^2}\right]. \tag{A.32}$$

For the simplicity of estimating this ratio, the authors of paper [13] considered $n_a \gg n_b$, so that

$$\frac{\omega_{We}}{\Omega} \sim \left(\frac{T}{Zn_a^2 U_H}\right) \ll 1 \tag{A.33}$$

as long as

$$T(\text{eV}) \ll (13.6\text{eV})Zn_a^2. \tag{A.34}$$

For example, for $Z = 2$ the above validity condition becomes

$$T(\text{eV}) \ll (27.2\text{eV})n_a^2 \tag{A.35}$$

and is satisfied for a broad range of temperatures, at which He II spectral lines are observed in plasmas.

References

[1] Griem H R and Shen K Y 1961 *Phys. Rev.* **122** 1490
[2] Griem H R 1964 *Plasma Spectroscopy* (New York: McGraw-Hill)
[3] Griem H R 1974 *Spectral Line Broadening by Plasmas* (Cambridge, MA: Academic)
[4] Lisitsa V S 1977 *Sov. Phys. Uspekhi* **122** 603
[5] Baranger M 1958 *Phys. Rev.* **111** 481 494
Baranger M 1958 *Phys. Rev.* **112** 855
[6] Kolb A C and Griem H R 1958 *Phys. Rev.* **111** 514
[7] Vidal C R, Cooper J and Smith E W 1970 *J. Quant. Spectrosc. Radiat. Transf.* **10** 1971**11** 263
[8] Sahal-Brechot S 1969 *Astron. Astrophys.* **1** 91
[9] Ispolatov Y and Oks E 1994 *J. Quant. Specrosc. Radiat. Transf.* **51** 129
[10] Oks E, Derevianko A and Ispolatov Y 1995 *J. Quant. Specrosc. Radiat. Transf.* **54** 307
[11] Oks E 2006 *Stark Broadening of Hydrogen and Hydrogenlike Spectral Lines in Plasmas: The Physical Insight* (Oxford: Alpha Science International)
[12] Oks E 1995 *Plasma Spectroscopy: the Influence of Microwave and Laser Fields* (Berlin: Springer)
[13] Sanders P and Oks E 2018 *J. Phys. Commun.* **2** 035033
[14] Oks E 2019 *Analytical Advances in Quantum and Celestial Mechanics: Separating Rapid and Slow Subsystems* (Bristol: IOP Publishing)
[15] Galitski V, Karnakov B, Kogan V and Galitski V Jr 2013 *Exploring Quantum Mechanics* (Oxford: Oxford University Press) problem 8.55.
[16] Kotkin G L and Serbo V G 1971 *Collection of Problems in Classical Mechanics* (Oxford: Pergamon) problem 2.3.
[17] Baryshnikov F F and Lisitsa V S 1981 *Sov. Phys. JETP* **53** 471

[18] Bureyeva L A and Lisitsa V S 2000 *A Perturbed Atom, Astrophysics and Space Physics Reviews* (Boca Raton, FL: CRC Press)
[19] Grützmacher K and Johannsen U 1993 *Spectral Line Shapes* vol 7, ed R Stamm and B Talin (New York: Nova Science) 139
[20] Ahmad R 1999 *Eur. Phys. J.* D **7** 123
[21] Wrubel T, Büscher S, Kunze H-J and Ferri S 2001 *J. Phys.* B **34** 461

IOP Publishing

Advances in X-Ray Spectroscopy of Laser Plasmas

Eugene Oks

Appendix B

Diagnostic of Langmuir solitons in plasmas by using hydrogenic spectral lines

Langmuir solitons are relatively strong Langmuir waves in plasmas—the waves having a certain spatial formfactor (see, for example book [1]). There are only very few theoretical papers on their spectroscopic diagnostics in plasmas—in distinction to a large number of works on various spectroscopic diagnostics of relatively weak Langmuir waves in plasmas and their successful implementation (see, e.g. books [2–4] and references therein).

In paper [5] the author calculated analytically the shape of satellites of dipole-forbidden lines in a spectrum *spatially-integrated* through a Langmuir soliton (or through a sequence of Langmuir solitons separated by a distance L). The dipole-forbidden lines are the characteristic feature of He and Li spectral lines or of the spectral lines of He-like and Li-like ions. In the profiles of these spectral lines, Langmuir waves can give rise to satellites of the dipole-forbidden components of these lines. The primary outcome of paper [5] (presented also in section 7.3 of book [2]) was the following.

In the case of Langmuir solitons, the peak intensity of the satellites of the dipole-forbidden lines can be significantly enhanced—by orders of magnitude—compared to the case of non-solitonic Langmuir waves. This specific feature allows distinguishing Langmuir solitons from non-solitonic Langmuir waves.

In distinction to the above method based on the dipole-forbidden spectral lines of He, Li, as well as He-like and Li-like ions, speaking of using hydrogenic spectral lines, one should mention that Hannachi *et al* [6] performed simulations for finding the effect of Langmuir solitons on the hydrogen Ly_α line. The outcome was an additional broadening. However, even at the low electron density $N_e = 10^{14}$ cm^{-3}, this additional broadening was very small compared to the Stark broadening by plasma microfields. Moreover, the additional broadening rapidly diminished with the increase of N_e—as a result, there would be practically no additional broadening at $N_e > 10^{15}$ cm^{-3}. In paper [7] Hannachi *et al* introduced into consideration additionally a magnetic field. Hannachi *et al* [7] performed simulations at the

doi:10.1088/978-0-7503-3375-7ch8

electron density $N_e = 10^{13}$ cm^{-3}. However, this electron density is unrealistically low for the modern tokamaks (applications to which were hoped for by the authors of paper [7]) and again, the additional broadening would rapidly diminish for more realistic values of the electron density (that is, for higher values of the electron density). Therefore, it appears highly questionable that the results by Hannachi *et al* [6, 7] could be of any use for the experimental diagnostics of Langmuir solitons. The results from paper [6] were also reproduced in one part of paper [8] by Stamm *et al*[1].

In paper [10], which we follow here, the author conducted a general study effects of Langmuir solitons on arbitrary spectral lines of hydrogen or hydrogen-like ions. Then by using the Ly-beta line as an example, he compared the main features of the profiles for the case of the Langmuir solitons with the case of the non-solitonic Langmuir waves of the same amplitude. He demonstrated how the line profiles depend on the amplitude of the Langmuir solitons and on their separation from each other within the sequence of the solitons.

Langmuir solitons (or a set of Langmuir solitons separated by a distance L) have the following spatial formfactor [1]:

$$F(x, t) = E(x)\cos \omega t, \quad E(x) = E_0/ch(x/\lambda), \quad \lambda \ll L. \tag{B.1}$$

Here

$$\omega = \omega_{\text{pe}} - 3Te/\left(2m_e\omega_{\text{pe}}\lambda^2\right), \tag{B.2}$$

where

$$\omega_{\text{pe}} = (4\pi e^2 N_e/m_e)^{1/2} \tag{B.3}$$

is the plasma electron frequency (m_e being the electron mass) and λ is the characteristic size of the soliton. A diagnostic of Langmuir solitons consists not only in finding experimentally the electric field oscillating at the frequency ~ω_{pe}, but also in ensuring that the spatial distribution of the amplitude corresponds to the formfactor $E(x)$ from equation (B.1).

The author of paper [10] started by considering the splitting of hydrogenic spectral lines at the fixed value of x. Then he averaged the result over the formfactor $E(x)$ from equation (B.1) to produce new results.

Blochinzew in his pioneering work of 1933 [11] considered the splitting of a model hydrogen line, consisting of just one Stark component, under a linearly-polarized electric field $\mathbf{E}_0 \cos \omega t$. He demonstrated that the model line splits up in satellites separated by $p\omega$ ($p = \pm 1, \pm 2, \pm 3, \ldots$) from the unperturbed frequency ω_0 of the spectral line:

[1] It should be noted that paper [8] by Stamm *et al* had a broad title 'Line shapes in turbulent plasmas'. Regrettably, the authors of paper [8] seem to be ignorant of dozens and dozens of theoretical and experimental papers on the subject of line shapes in turbulent plasmas that started in Sholin's group as early as in the 1970s and continued by various theoretical and experimental groups around the world through 2017—see, e.g. paper [9], book [2] and references from paper [9] and book [2].

$$S(\Delta\omega/\omega) = \sum_{p=-\infty}^{+\infty} \left[J_p^2(X_k\varepsilon)\right](\delta(\Delta\omega/\omega) - p), \tag{B.4}$$

where $J_p(u)$ are the Bessel functions, ε is the scaled amplitude of the field:

$$\varepsilon = 3\hbar E_0/(2Z_r m_e e\omega). \tag{B.5}$$

Here Z_r is the nuclear charge of the radiating atom/ion and

$$X_k = nq - n_0 q_0, \tag{B.6}$$

where n, q and n_0, q_0 are the principal and electric quantum numbers of the upper and lower energy levels, respectively, involved in the radiative transition. From the physical point of view, the greater the product $X_k\varepsilon$, the larger is the phase modulation of the atomic oscillator. In paper [12] Blochinzew's result was generalized to profiles of real, multicomponent hydrogenic spectral lines in the 'reduced frequency' scale as follows (presented later also in book [4], section 3.1)

$$S(\Delta\omega/\omega) = \sum_{p=-\infty}^{+\infty} I(p, \varepsilon)\delta(\Delta\omega/\omega) - p, \tag{B.7}$$

where

$$I(p, \varepsilon) = \left[f_0\delta_{p0} + 2\sum_{k=1}^{k_{\max}} f_k J_p^2(X_k\varepsilon)\right] / \left(f_0 + 2\Sigma f_k\right). \tag{B.8}$$

Here f_0 is the total intensity of all central Stark components, f_k is the intensity of the lateral Stark component with the number $k = 1, 2, \ldots, k_{\max}$.

In the typical case of the strong modulation ($X_k\varepsilon \gg 1$), from equations (B.4), (B.7), (B.8) it is seen that there could be numerous satellites of significant intensities. Often the situation is such that the individual satellites merge together by broadening mechanisms. In this situation only the envelope of these satellites can be observed. The most intense part of the satellites envelope has the shape of the Airy function, as shown in paper [12] and reproduced in book [4], section 3.1. Based on these analytical results, the following practical formulas have been derived and presented in paper [12] and reproduced in book [3] (section 3.1) for the position $p_{\max}$ of the satellite having the maximum intensity (and thus corresponding to the experimental peak)

$$p_{\max}(a) = a + (a/2)^{1/3}d_{\mathrm{Ai}} = a - 0.809(a)^{1/3}, \quad a = X_k\varepsilon, \tag{B.9}$$

where $d_{\mathrm{Ai}} = -1.019$ is the first zero of the derivative of the Airy function.

In paper [10] the author started the averaging over the formfactor $E(x)$ from equation (B.1) by substituting $E(x)$ into the argument of the Bessel function in equation (B.4) and integrating over x from $-\lambda$ to λ, or equivalently

$$f(p, a, b) = (1/b) \int\int_{-b/2}^{b/2} dy J_p^2[a/ch(y)], \tag{B.10}$$

where he denoted

$$b = L/\lambda, \quad y = x/\lambda. \tag{B.11}$$

Since the maximum intensity has the satellite at the position $p_{\max}(a)$ given by equation (B.9), then its spatially integrated intensity from equation (B.10) is $I = f[p_{\max}(a), a, b]$. Figure B1 shows I versus b for $a = 10$ (solid line), $a = 15$ (dashed line), and $a = 20$ (dotted line). It is seen that the integrated intensity of the most prominent satellite decreases as either a increases (e.g. the field amplitude E_0 increases) or as b increases (i.e. the distance L between Langmuir solitons in the sequence increases).

Figure B2 presents a three-dimensional plot of the spatially integrated intensity of the most prominent satellite versus both a and b.

Figure B3 shows a three-dimensional plot of the ratio $f[p_{\max}(a), a, b]/f[0, a, b]$ versus a and b. This is the ratio of the spatially integrated intensity of the most prominent satellite to the spatially integrated intensity of the 'zeroth' satellite, the latter being the intensity at the unperturbed position of the one-component spectral line. It is seen that this ratio is generally a non-monotonic function of the scaled amplitude a of the solitons electric field.

Then the author of paper [10] proceeded to real, multi-component hydrogenic spectral lines. As an example, he utilized the Ly-beta line in the observation perpendicular to the solitons electric field.

Figure B4 presents the profile of the Ly-beta line versus the scaled distance $\Delta\omega/\omega$ from the unperturbed position of this line for the (differently) scaled amplitude $\varepsilon = 3\hbar E_0/(2Z_r m_e e\omega) = 1$ and the scaled distance $b = L/\lambda = 2$ between the Langmuir solitons in the sequence (solid line). Also shown is the corresponding profile for the case of the non-solitonic Langmuir waves for the same value of $\varepsilon = 1$ (dashed line).

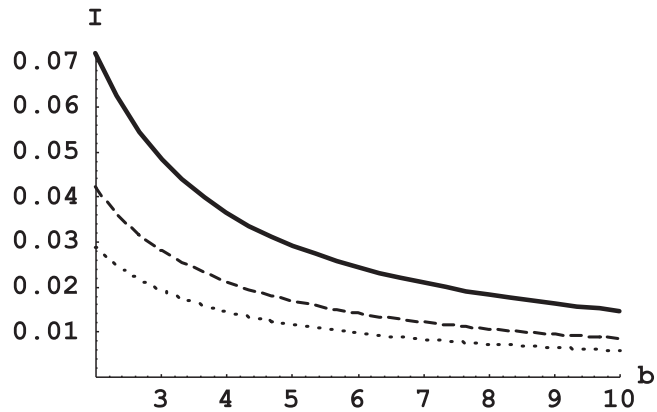

Figure B1. Spatially integrated intensity I of the most prominent satellite versus the scaled distance $b = L/\lambda$ of Langmuir solitons in the sequence for three values of the scaled amplitude $a = 3\hbar X_k E_0/(2Z_r m_e e\omega)$ of the solitons electric field: $a = 10$ (solid line), $a = 15$ (dashed line), and $a = 20$ (dotted line) [10].

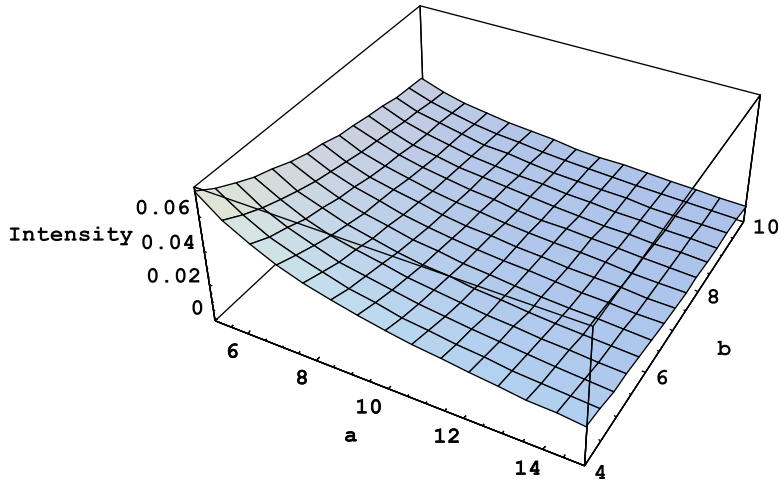

Figure B2. Spatially integrated intensity of the most prominent satellite versus the scaled amplitude $a = 3\hbar X_k E_0/(2Z_r m_e e\omega)$ of the solitons electric field and versus the scaled distance $b = L/\lambda$ of Langmuir solitons in the sequence [10].

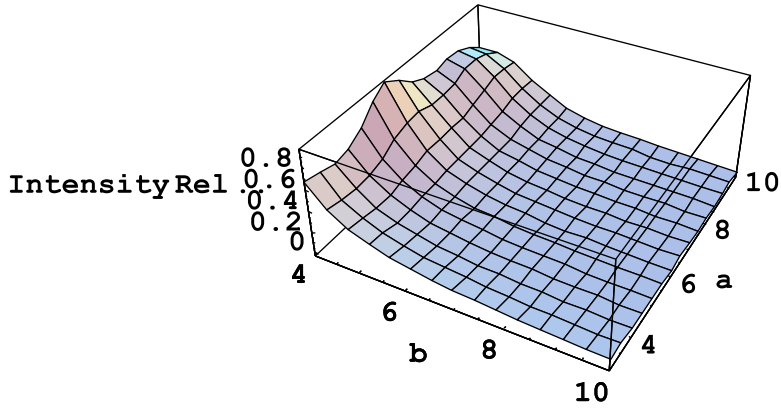

Figure B3. The ratio $f[p_{\max}(a), a, b]/f[0, a, b]$ of the spatially integrated intensity of the most prominent satellite to the spatially integrated intensity of the 'zeroth' satellite versus the scaled amplitude $a = 3\hbar X_k E_0/(2Z_r m_e e\omega)$ of the solitons electric field and versus the scaled distance $b = L/\lambda$ of Langmuir solitons in the sequence [10].

The direction of the observation is perpendicular to vector $\mathbf{E}_0$. The profiles are continuous (rather than being a set of satellites isolated from each other) because additional broadening mechanisms (the Stark broadening by plasma microfields and the Doppler broadening) were taken into account in the amount of $\delta\omega = 2\omega$. The latter relation could be satisfied, for example, in plasmas of multi-charged ions produced by a powerful Nd-glass laser, where at the surface of the critical density, the electron density is $N_e = 10^{21}$ cm^{-3} (or slightly higher due to relativistic effects) and the temperature would be up to $T \sim 10^3$ eV.

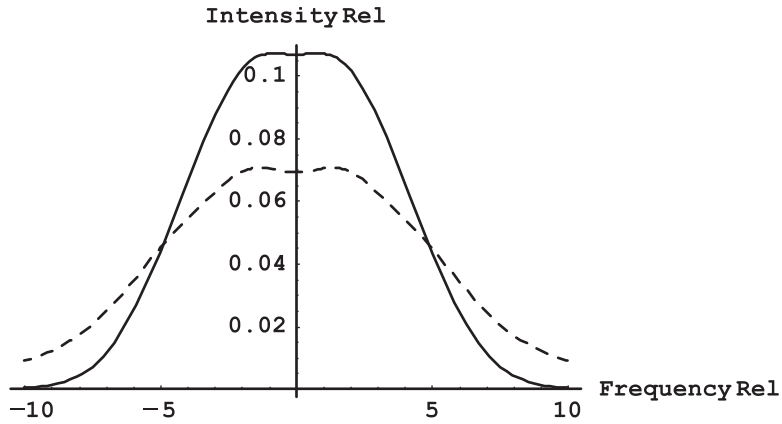

Figure B4. The profile of the Ly-beta line versus the scaled distance $\Delta\omega/\omega$ from the unperturbed position of this line for the (differently) scaled amplitude $\varepsilon = 3\hbar E_0/(2Z_i m_e e\omega) = 1$ and the scaled distance $b = L/\lambda = 2$ of Langmuir solitons in the sequence (solid line) [10]. Also shown is the corresponding profile for the case of the non-solitonic Langmuir waves for the same value of $\varepsilon = 1$ (dashed line). The direction of the observation is perpendicular to vector $\mathbf{E}_0$.

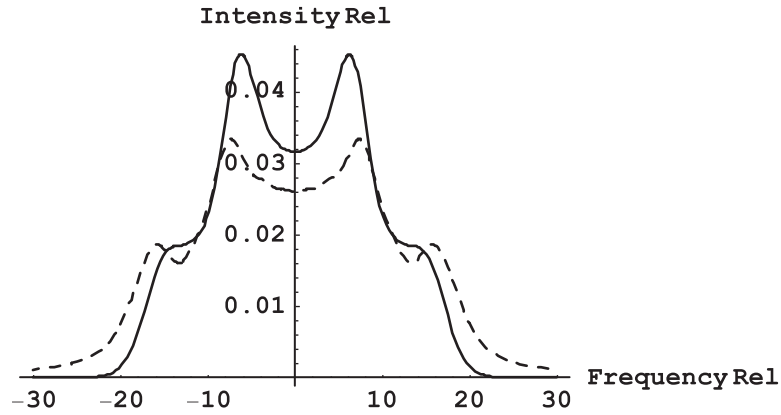

Figure B5. The same as figure B4, but for stronger Langmuir waves, corresponding to $\varepsilon = 3$ [10].

It is seen that in the case of the solitons, the profile is narrower than in the non-solitonic case. It is also seen that both profiles have practically the bell-shape without any significant features.

Figure B5 shows the same as figure B4, but for stronger Langmuir waves, corresponding to $\varepsilon = 3$. Both profiles have features. Namely, in the non-solitonic case (dashed line), the profile has two maxima both in the red and blue sides. In the case of solitons, the primary maximum in each side remains, but the secondary maximum in each side transforms into a shoulder.

Figure B6 shows the same as figure B5, but for even stronger Langmuir waves, corresponding to $\varepsilon = 6$. Both profiles have more features than in figure B5: three maxima both in the red and blue sides. In the case of solitons, the second maximum

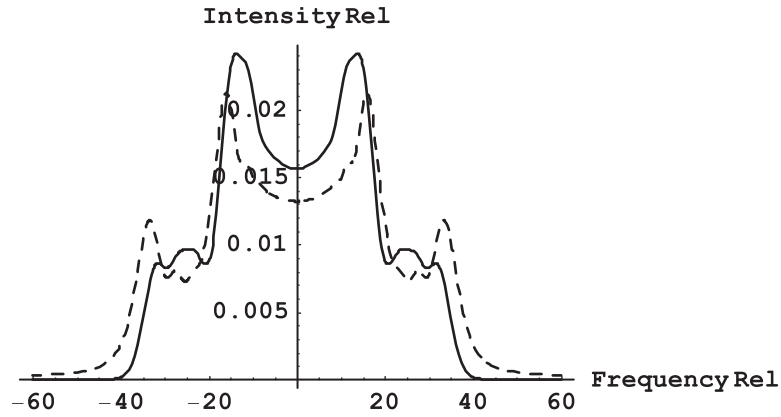

Figure B6. The same as figure B5, but for even stronger Langmuir waves, corresponding to $\varepsilon = 6$ [10].

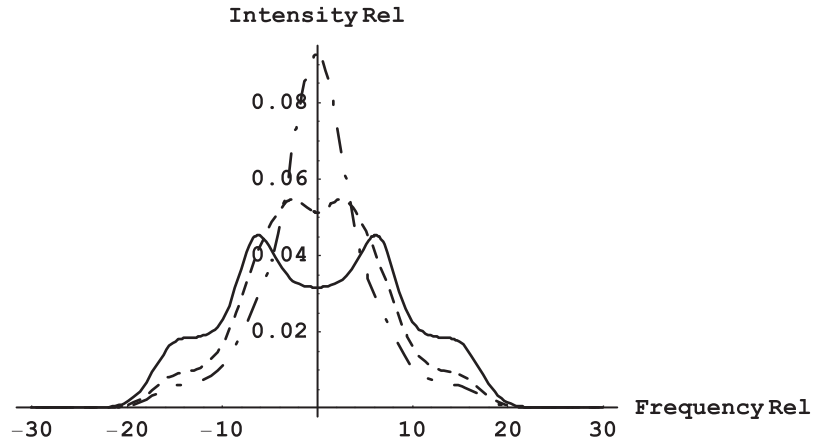

Figure B7. Dependence of the Ly-beta profiles for the case of the Langmuir solitons on the scaled distance $b = L/\lambda$ between the Langmuir solitons in the sequence: for $b = 2$ (solid line), $b = 4$ (dashed line), and $b = 6$ (dash-dotted line) [10].

in each side is more pronounced than for the non-solitonic case. For the third maximum the situation is opposite: the case of solitons, the third maximum is less pronounced than for the non-solitonic case.

Then the author of paper [10] exhibited how the Ly-beta profiles for the case of the Langmuir solitons, depend on the scaled distance $b = L/\lambda$ between Langmuir solitons in the sequence. In figure B7 the Ly-beta profiles corresponding to $\varepsilon = 3$, are presented for $b = 2$ (solid line), $b = 4$ (dashed line), and $b = 6$ (dash-dotted line). It is seen that as the scaled distance $b = L/\lambda$ between Langmuir solitons in the sequence increases, the features (such as maxima, minima, shoulders) gradually disappear.

The above shows that the diagnostic of Langmuir solitons, while employing, for example, the Ly-beta line, can be based on the following feature. In the non-solitonic case, there could be distinct secondary maxima in each wing of the line, whereas in

the case of solitons the would-be secondary maxima look more or less like shoulders —see figures B5 and B6, and the solid line in figure B7.

In summary, in paper [10] the author suggested using the following manifestations of Langmuir solitons as the diagnostic tool. For the case of the Langmuir solitons, some maxima in the line profiles become less pronounced or even transform into shoulders—compared to the non-solitonic Langmuir waves of the same amplitude. Also, as the amplitude of the Langmuir solitons increases, more features (such as maxima and minima) appear in the line profiles. However, when the separation between the solitons within their set increases, there are less features in the line profiles.

These manifestations can be used for the experimental determination of the amplitude of the Langmuir solitons and of their separation from each other in their sequence.

References

[1] Kadomtsev B B 1982 *Collective Phenomena in Plasma* (Oxford: Pergamon)
[2] Oks E 2017 *Diagnostics of Laboratory and Astrophysical Plasmas Using Spectral Lines of One-, Two-, and Three-Electron Systems* (Singapore: World Scientific)
[3] Griem H R 1997 *Principles of Plasma Spectroscopy* (Cambridge: Cambridge University Press)
[4] Oks E 1995 *Plasma Spectroscopy: The Influence of Microwave and Laser Fields* (Berlin: Springer)
[5] Oks E 2017 *J. Phys. Conf. Ser.* **810** 012006
[6] Hannachi I, Stamm R, Rosato J and Marandet Y 2016 *Europhys. Lett.* **114** 23002
[7] Hannachi I, Meireni M, Rosato J, Stamm R and Marandet Y 2018 *Contrib. Plasma Phys.* **58** 583
[8] Stamm R *et al* 2017 *Eur. Phys. J.* D **71** 68
[9] Oks E *et al* 2017 *Opt. Express* **25** 1958
[10] Oks E 2019 *Atoms* **7** 25
[11] Blochinzew D I 1933 *Phys. Z. Sov. Union* **4** 501
[12] Oks E 1984 *Sov. Phys. Doklady* **29** 224

IOP Publishing

Advances in X-Ray Spectroscopy of Laser Plasmas

Eugene Oks

Appendix C

Profiles of hydrogenic spectral lines under stochastic electric fields of plasma turbulence: applications to diagnostics of the Langmuir turbulence

At sufficiently high electron densities $N_e \gg 10^{18}$ cm^{-3}, the Langmuir turbulence can cease to be quasimonochromatic and rather represents a broadband electric field with the peak intensity at the plasma electron frequency ω_{pe}, where

$$\omega_{pe} = (4\pi e^2 N_e/m_e)^{1/2} \tag{C.1}$$

(here e and m_e are the electron charge and mass, respectively). This happens mostly due to electron collisions. The electric field of the Langmuir turbulence becomes multi-mode and can be even stochastic.

In this scenario the Langmuir turbulence can lead to a broadening of hydrogenic spectral lines. In the 1970s, this effect was pointed out by Sholin [1] and then developed in more detail by Oks and Sholin [2]. This effect was used for interpreting some experimental results in papers [3–5].

A further theoretical study related to this physical situation was performed by Gavrilenko [6] in 1996. Specifically, he considered modifications of profiles of hydrogen spectral lines under a multi-mode *non-monochromatic* linearly-polarized electric field[1].

In paper [6] Gavrilenko obtained his results for the case where the *power spectrum* of the stochastic electric field is *Lorentzian*. In paper [8] the author extended Gavrilenko's results to the scenario where the *power spectrum* of the stochastic

[1] It should be mentioned that in 1958, Lifshitz [7] studied theoretically the influence of a multi-mode *monochromatic* linearly-polarized electric field on a model hydrogen line, consisting of just one Stark component. That study was not relevant to the problem of broadening hydrogenic spectral lines by the multi-mode *non-monochromatic* electric field of the Langmuir turbulence in plasmas of sufficiently high electron densities.

doi:10.1088/978-0-7503-3375-7ch9

electric field is *Gaussian*. In addition, he studied theoretically the general case of hydrogenlike spectral lines—rather than only hydrogen spectral lines considered by Gavrilenko [6].

In paper [8] the author first deduced a general analytical result for the correlation function, whose Fourier transform determines the shape of the spectral line. Then he demonstrated that when the power spectrum of the field is sufficiently broad, hydrogenic line profiles are significantly narrower in his case compared to Gavrilenko's case—despite the power spectra of the field in both cases having the same full width at half maximum (FWHM). Below are a few more details.

Following notation by Gavrilenko [6], the correlation function of the field can be represented in the form

$$\{\mathbf{E}(t)\mathbf{E}(t+\tau)\}_{\text{av}} = BG(\tau), \qquad B = \{\mathbf{E}^2\}_{\text{av}} \tag{C.2}$$

where $G(\tau)$ is a correlation coefficient.

In paper [8] the author considered the case where the correlation coefficient is

$$G(\tau) = \exp(-\tau^2/g^2)\cos\omega\tau, \tag{C.3}$$

so that the *power spectrum* of the field $\mathbf{E}(t)$ has the *Gaussian* form. The author of paper [8] introduced the following notation

$$b = C_{\alpha\beta}^2 B, \tag{C.4}$$

where

$$C_{\alpha\beta} = 3(n_a q_\alpha - n_b q_\beta)/(2Z). \tag{C.5}$$

In equation (C.5), Z is the nuclear charge; n and q are the principal and electric quantum numbers, respectively, of the upper (a, α) and lower (b, β) Stark sublevels involved in the radiative transition ($q = n_1 - n_2$, where n_1 and n_2 are the parabolic quantum numbers). In equations (C.4), (C.5), and below, the atomic units are used:

$$\hbar = e = m_e = 1.$$

Further, the author of paper [8] denoted as D the detuning in the frequency scale from the unperturbed position of the spectral line:

$$D = \Delta\Omega - \delta_{ab}. \tag{C.6}$$

Below are three figures from paper [8] as the illustrations of the analytical results from paper [8] for the correlation coefficient of the electric field given by equation (C.3). In all figures below, the quantities b, g, and D are measured in units of the carrier frequency ω (for example, $D = (\Delta\Omega - \delta_{ab})/\omega$).

Figure C1 exhibits the profile of any Stark component for $b = 20$ and $g = 0.2$ (bold solid line). Also shown is the Lorentzian of $\text{FWHM}_\text{L} = \pi^{1/2} bg$ (dashed line) and the Gaussian of $\text{FWHM}_\text{G} = 2(2b \ln 2)^{1/2}$ (thin solid line). It is seen that the bulk of the profile is close to the Lorentzian shape and that in the wings there occurs the transition to the Gaussian shape. This kind of spectral line shape is a counter-intuitive result.

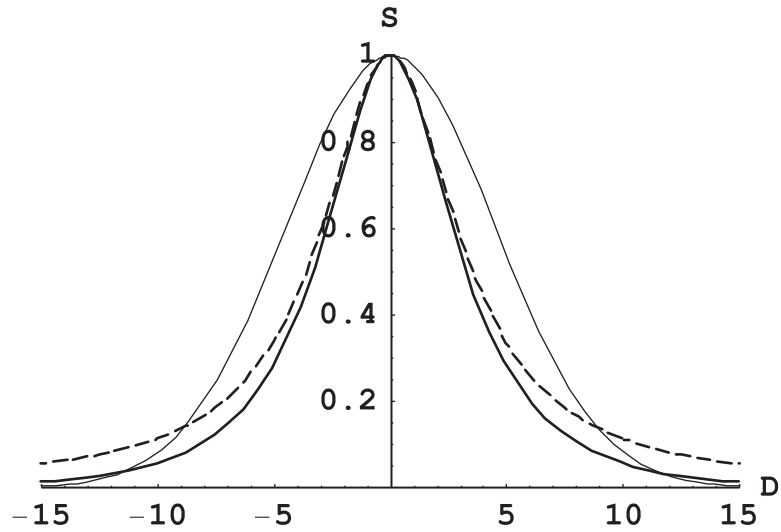

Figure C1. The calculated profile of any Stark component for $b = 20$ and $g = 0.2$ (bold solid line) versus the scaled dimensionless detuning $D = (\Delta\Omega - \delta_{ab})/\omega$. Also shown is the Lorentzian of $\mathrm{FWHM_L} = \pi^{1/2} bg$ (dashed line) and the Gaussian of $\mathrm{FWHM_G} = 2(2b \ln 2)^{1/2}$ (thin solid line) [8]. The profiles are peak-normalized. The quantities g and b from equations (C.3) and (C.4) are in units of the carrier frequency ω. Reprinted from [8], copyright 2020, with permission from Elsevier.

In figure C2, the calculated three-dimensional plot demonstrates the transformation of the profile of any Stark component as the quantity g varies, while the quantity $b = 30$. It is seen that as the quantity g increases, so does the width of the profile

In figure C3 the calculated three-dimensional plot demonstrates the transformation of the profile of any Stark component as the quantity b varies, while the quantity $g = 0.2$. It is seen that as the quantity b increases, so does the width of the profile.

From figures C2 and C3 one can clearly see that as b or g increases, so does the width of the profile of any Stark component. This is consistent with the analytical results from paper [8].

By analyzing the corresponding theoretical profiles of the hydrogenic Ly-beta line, the author of paper [8] proposed a *new diagnostic method allowing for the first time not only to measure experimentally the average field* of the Langmuir turbulence in dense plasmas, but also to find out *the information on the power spectrum* of the Langmuir turbulence. This diagnostic method is not limited to using the Ly-beta line of hydrogenic atoms/ions. This method would work while using other intense hydrogenic spectral lines that, like the Ly-beta line, do not have the central Stark components. Examples are the hydrogenic spectral lines Ly-delta, Balmer-beta, and Balmer-delta. Thus, this method could serve as a tool for the experimental testing of the field correlation function.

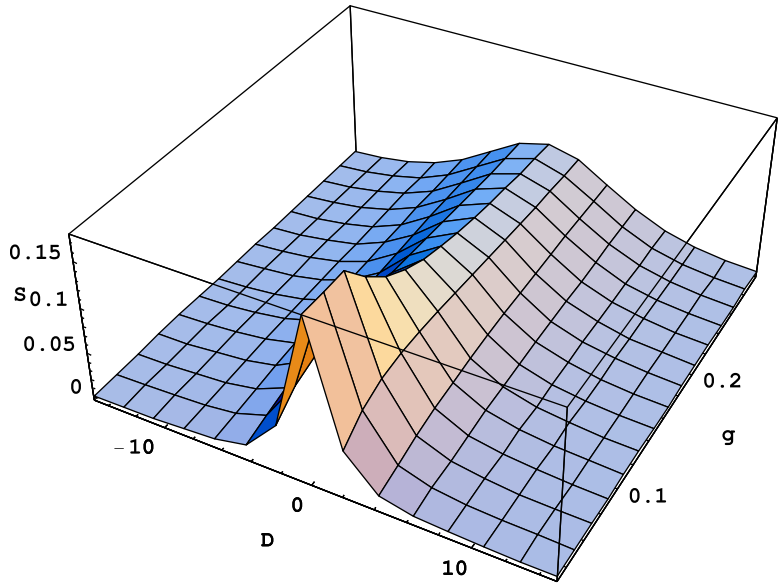

Figure C2. The calculated three-dimensional plot showing the transformation of the profile of any Stark component as the quantity g varies, while the quantity $b = 30$ [8]. The quantities g and b from equations (C.3) and (C.4) are in units of the carrier frequency ω. Reprinted from [8], copyright 2020, with permission from Elsevier.

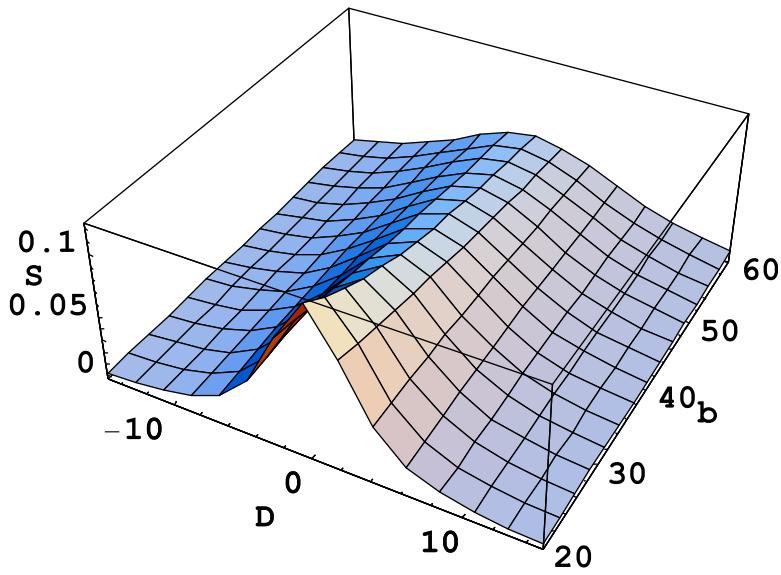

Figure C3. The calculated three-dimensional plot showing the transformation of the profile of any Stark component as the quantity b varies, while the quantity $g = 0.2$ [8]. The quantities g and b from equations (C.3) and (C.4) are in units of the carrier frequency ω. Reprinted from [8], copyright 2020, with permission from Elsevier.

References

[1] Sholin G V 1970 *Sov. Phys. Doklady* **15** 1040
[2] Oks E and Sholin G V 1975 *Sov. Phys. JETP* **41** 482
[3] Zakatov L P, Plakhov A G, Shapkin V V and Sholin G V 1971 *Sov. Phys. Doklady* **16** 451
[4] Karfidov D M and Lukina N A 1997 *Phys. Lett.* A **232** 443
[5] Oks E 2016 *J. Phys. B: At. Mol. Opt. Phys.* **49** 065701
[6] Gavrilenko V P 1996 *Pis'ma v Zh. Tech. Phys. (Sov. Phys. Tech. Phys. Lett.)* **22** 23 (in Russian)
[7] Lifshitz E V 1958 *Sov. Phys. JETP* **26** 570
[8] Oks E 2020 *Spectrochim. Acta* B **167** 105815